ACS APPLIED MATERIALS & INTERFACES

Research Article

www.acsami.org

Cementation of Colloidal Particles on Electrodes in a Galvanic Microreactor

Linda Jan, Christian Punckt, and Ilhan A. Aksay*

Department of Chemical and Biological Engineering, Princeton University, Princeton, New Jersey 08544, United States

Supporting Information

ABSTRACT: We have studied the processes leading to the cementation of colloidal particles during their autonomous assembly on corroding copper electrodes within a Cu−Au galvanic microreactor. We determined the onset of particle immobilization through particle tracking, monitored the dissolution of copper as well as the deposition of insoluble products of the corrosion reactions in situ, and showed that particle immobilization initiated after reaction products (RPs) began to deposit on the electrode substrate. We further demonstrated that the time and the extent of RP precipitation and thus the strength of the particle−substrate bond could be tuned by varying the amount of copper in the system and the microreactor pH. The ability to cement colloidal particles at locations undergoing corrosion illustrates that the studied colloidal assembly approach holds potential for applications in dynamic material property adaptation.

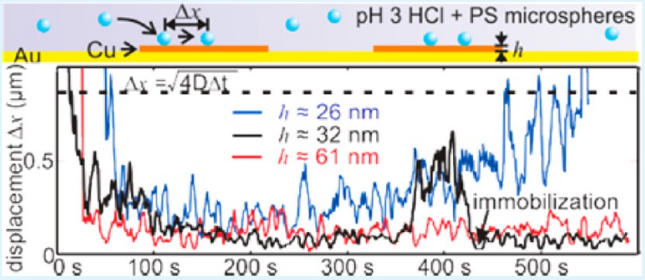

KEYWORDS: *electrochemistry, colloidal particles, material processing, galvanic corrosion, cementation, reaction products*

INTRODUCTION

Colloidal crystals have a variety of potential uses, including sensors[1−3] and photonic devices.[4−6] Employing colloidal crystals in such systems requires the controlled aggregation of the colloidal particles into well-defined patterns, followed by their immobilization on a substrate so that the assembly is not destroyed during further use or processing. Electrokinetics can be used to guide the aggregation and patterning of colloidal crystals in a fast and versatile manner, and the speed and direction of colloidal particles can be controlled by electric fields.[7−12] Recent research in this area has focused on autonomous transport and aggregation of colloidal particles in galvanic cells during the catalytic decomposition of hydrogen peroxide on pairs of dissimilar metal electrodes.[13] However, in these approaches, the fundamentals of the adherence of the particles onto the substrate after patterning have not been addressed.

We showed recently that, during the galvanic corrosion of copper microelectrodes embedded in a gold substrate and immersed in an acidic suspension (pH 3 hydrochloric acid) of sulfate-decorated polystyrene (PS) particles (Cu−Au galvanic microreactor) (Figure 1a), predetermined patterns of two-dimensional colloidal single crystals with a defined orientation could be cemented onto the electrode substrate (Figure 1b).[14] While the directed long-range transport of the colloidal particles to the copper electrode by reaction-induced fluid flow and electrophoresis[14,15] and their subsequent crystallization by electrohydrodynamic[7,14,16] and electroosmotic flow[16,17] have been well-understood, the effect of the reaction parameters on the cementation of a monolayer of colloidal particles onto the substrate required further study. Preliminary evidence indicated that particle adherence correlated with the presence of reaction products (RPs) on the substrate and that the quantity of RPs increased with the amount of copper in the microreactor.[14] Therefore, we hypothesized that RPs may be responsible for the "cementation" of the colloidal particles onto the electrode.

RPs that may form in the microreactor during copper corrosion can be identified by examining the chemistry of copper corrosion in aqueous chloride media. It has been established that, in the presence of chloride ions, the dissolution of copper proceeds first through the formation of an insoluble cuprous chloride (CuCl) film[18−21]

$$Cu + Cl^- \leftrightharpoons CuCl + e^- \quad (1)$$

which can form water-soluble complexes with chloride and dissolve into the electrolyte:[18,21]

$$CuCl + Cl^- \leftrightharpoons CuCl_2^- \quad (2)$$

At low chloride concentrations, a significant amount of cupric ions can form according to[18]

$$CuCl_2^- \leftrightharpoons Cu^{2+} + 2Cl^- + e^- \quad (3)$$

Lastly, $CuCl_2^-$ reacts with water in a homogeneous reaction to form Cu_2O precipitates:[20]

Received: April 17, 2013
Accepted: June 14, 2013
Published: June 14, 2013

dx.doi.org/10.1021/am4014117 | ACS Appl. Mater. Interfaces 2013, 5, 6346−6353

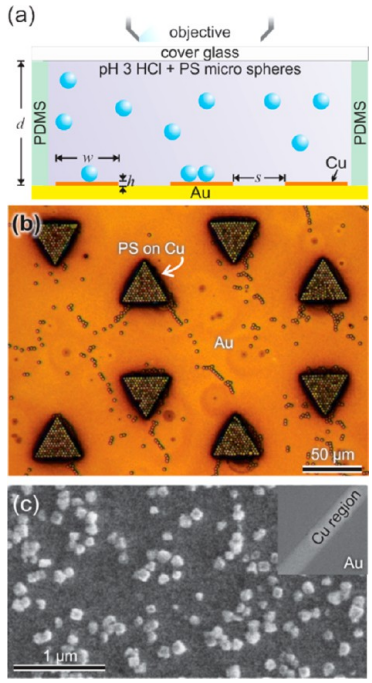

Figure 1. (a) Schematic of the galvanic microreactor. (b) Patterned and crystalline two-dimensional colloidal aggregates adherent to triangular copper electrodes, which are lowered compared to the gold electrode, imaged after rinsing and drying of the sample. Particles distributed on the gold substrate have been deposited there during rinsing and drying. Parameters: copper triangle electrodes side length ≈40 μm with ≈60 μm edge-to-edge separation, 0.11 vol % PS particles in pH 3 HCl electrolyte. This image is reproduced from Jan et al.[15] (c) SEM image of the "copper region" following a reaction with pH 3 HCl showing cubic crystallite RPs. (Inset) Low-magnification SEM image of the same electrode showing both copper and gold regions.

$$2CuCl_2^- + H_2O \leftrightharpoons Cu_2O + 2H^+ + 4Cl^- \quad (4)$$

Additional reactions may also take place to form other insoluble RP species (e.g., $Cu_2(OH)_3Cl$).[20,22] Oxidation reactions 1 and 3 on the copper electrode are electrically balanced by the reduction of dissolved oxygen to form hydrogen peroxide, which occurs primarily on the gold cathode:[23]

$$O_2 + 2H^+ + 2e^- \leftrightharpoons H_2O_2 \quad (5)$$

Thus, insoluble RPs in the microreactor can potentially be constituted of a CuCl surface film forming according to eq 1, of Cu_2O precipitating via eq 4, or of more complex species, such as copper hydroxychloride or other copper minerals.[20] In our previous study, ex situ examination of the RPs with a scanning electron microscope (SEM) (Figure 1c) and electron backscattered spectroscopy revealed that, by the end of the reactions (i.e., after electrode drying), the RP was primarily Cu_2O.[14] Further, since the colloidal particle aggregates "anneal" into crystalline structures prior to adherence, we inferred that particle adherence occurred at a later stage of the galvanic corrosion process. We hypothesized that, as the reactions progressed, a decrease in chloride concentration (due to eqs 1 and 2) and an increase in electrolyte pH (due to eq 5) shifted the chemical equilibrium in the microreactor, effecting Cu_2O precipitation described by eq 4 and leading to particle cementation through RP deposition on electrodes and colloidal particles. However, the type of RP responsible for particle cementation in situ as well as the relationship between its formation, particle cementation, and the chemical changes in the microreactor remained unknown and required further investigation.

In this study, we show that, by monitoring particle motion, aggregation, and cementation on the electrode substrate in situ, we are able to relate the observed particle dynamics and eventual immobilization to the onset of RP precipitation and deposition. We analyze how increasing amounts of copper in the microreactor affect colloidal particle dynamics as well as RPs formation, and we explain how changing chemical equilibria during the corrosion of copper can be responsible for RPs precipitation and, consequently, particle cementation. Finally, we show that a sufficient shift in the microreactor chemistry can be achieved by increasing the amount of copper or by raising the initial pH, illustrating that particle cementation can be controlled by variation of these parameters. We expect our findings concerning the adherence of matter at precise locations in response to a chemical stimulus, such as locally occurring corrosion reactions, to hold potential for the development of self-healing systems and methods to manufacture materials autonomously.

METHODS

The Cu–Au galvanic microreactor consisted of a patterned array of copper anodes surrounded by a continuous gold cathode, as shown schematically in Figure 1a. We fabricated the galvanic electrodes by first depositing a 10 nm titanium film, followed by a 100 nm gold film on a silicon wafer using an e-beam evaporator (Denton DV-502A, Denton Vacuum, Moorestown, NJ). A copper film was then electrolessly plated onto the gold at 25 °C, using a solution of 1.5 g of copper sulfate, 7.0 g of potassium sodium tartrate (chelating agent), 2.0 g of sodium hydroxide (pH adjustment), and 5 mL of formaldehyde (reducing agent) in 50 mL of deionized (DI) water. Plating times were varied depending on the desired copper film thickness (h). Next, we used standard photolithography to pattern photoresist (AZ(R) 5214-E, Clariant Corp., Somerville, NJ) on top of the copper. Following photolithography, the electrodes were etched in ~0.1 M nitric acid to form patterns of the copper thin film on a gold substrate. The specific design used in this study consisted of long copper lines of width w separated at a distance s, as shown in Figure 1a, whereas, in our previous studies,[14,15] triangular anodic copper trenches (Figure 1b) were used to effect the formation of single crystalline arrays. We measured h using a profilometer (P-15, KLA Tencor, Milpitas, CA). Prior to each experiment, the electrodes were etched for ≈5 s in pH 3 HCl electrolyte to minimize surface oxide layers.

The galvanic microreactor was assembled by placing a circular poly(dimethylsiloxane) (PDMS) spacer of $d \approx 350$ or 510 μm in thickness and ≈7 mm in inner diameter on top of the galvanic electrode. The reactions were initiated by filling the chamber with a reaction solution (pH 3, pH 3.5, or pH 3.5 HCl with added sodium chloride) and enclosing it with a microscope cover glass. For particle aggregation experiments, surfactant-free, sulfate-decorated PS colloidal microspheres of ≈2.3 μm in diameter (lot 53977A, Invitrogen, Eugene, OR) were suspended in the reaction solutions at particle concentrations of 0.008–0.4 vol %. In situ observations were made using reflection bright field microscopy (Zeiss Axioplan 2, Carl Zeiss MicroImaging, Inc., Thornwood, NY) and recorded using a 12-bit digital CCD camera (Zeiss AxioCam HRc, Carl Zeiss MicroImaging, Inc., Thornwood, NY). The reactions were terminated by immersing the electrodes in a bath of DI water, gently swirling the electrode for ≈10 s, followed by blow drying with nitrogen. The electrophoretic mobility of PS particles suspended in pH 3 HCl electrolyte was obtained using a Coulter DELSA 440SX unit (Beckman Coulter, Inc., Miami, FL) and converted to a ζ-potential of −44 ± 3 mV using the method of O'Brien and White.[24] We expect the ζ-potential of PS particles suspended in pH 3.5 HCl electrolytes to be more negative.

dx.doi.org/10.1021/am4014117 | ACS Appl. Mater. Interfaces 2013, 5, 6346–6353

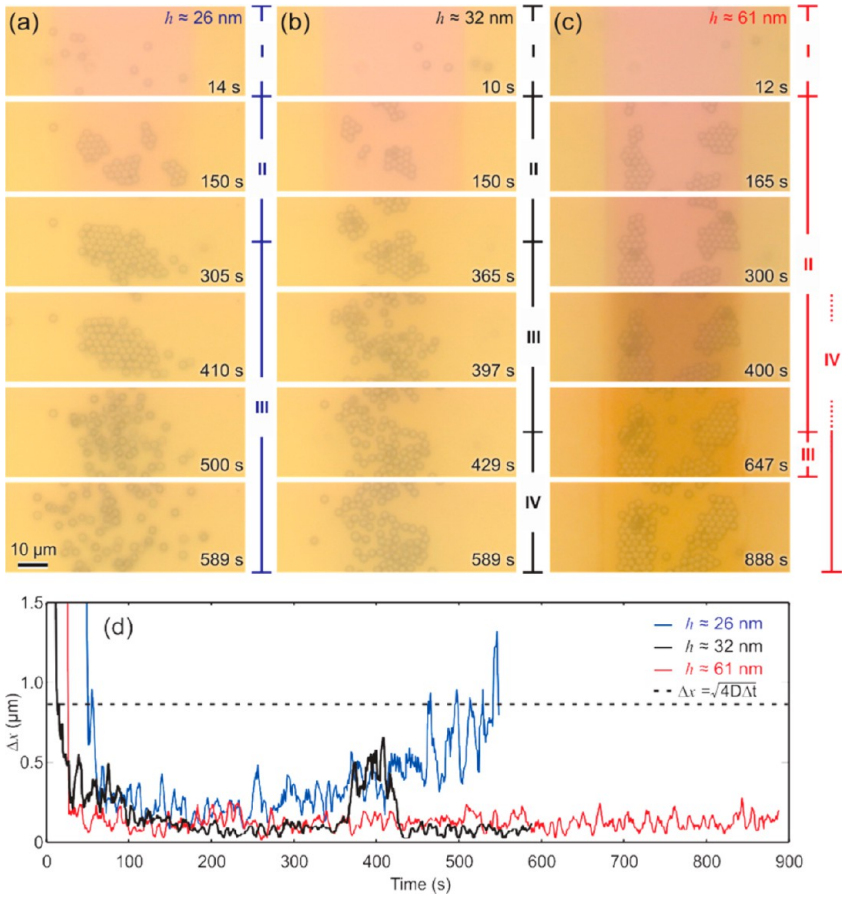

Figure 2. Motion of particles on the electrode surface in situ during reaction with a dilute (0.008 vol %) particle suspension in pH 3 HCl electrolyte. Reactions were conducted for varying h: (a) $h \approx 26$ nm, (b) $h \approx 32$ nm, and (c) $h \approx 61$ nm. Other reactor dimensions (see Figure 1a) are kept constant: $w \approx 50$ μm, $s \approx 950$ μm, and $d \approx 350$ μm). Onset of the four stages of colloidal behavior is indicated schematically for the different experimental conditions. (d) Particle displacement Δx during a time interval of $\Delta t = 1$ s for three representative particles at indicated values of h. The dashed black line indicates the displacement expected for a particle's Brownian motion Δx_{diff}. The measurement noise corresponds to the spatial resolution of our imaging system.

For the particle tracking experiments, in situ images of the colloidal particles were recorded at 1 Hz. The centers of the particles were identified manually by marking them in a magnified view of the image using MATLAB. The locations were stored as a function of time, and the projected lateral displacements of the particles Δx during the 1 s time step were determined using an algorithm written in house. Δx was smoothened with a linear Savitzky–Golay[25] filter (using a 5 data point window) and plotted against reaction time. The measurement error for particle centers identified this way was roughly 1 pixel, or $\approx$0.13 μm.

For the color analysis experiments, color bright-field images of the galvanic electrodes were recorded at 1 Hz during reactions without colloidal particles. In a manner similar to the method described by Punckt et al.,[26] we monitored and analyzed the red, green, and blue (RGB) color channels in the recorded images from both copper and gold regions during the reactions. We determined that the blue color channel was the most sensitive to copper electrode thickness changes and exhibited the most linear response with varying electrode thicknesses. Thus, the time evolution of the normalized values of the blue color channel was used to assess copper film corrosion and RPs deposition.

To examine the electrode surface underneath the colloidal particles when adherent particles were present, we removed the particles by briefly ($\approx$5–10 s) ultrasonicating the electrode in DI water and drying with nitrogen gas. Afterward, the electrode surfaces were examined using an SEM (VEGA 1, Tescan, Czech Republic) at 20 kV acceleration voltage. Energy-dispersive X-ray spectroscopy (EDS) was performed at 5 kV accelerating voltage using an INCA x-act detector (Oxford Instruments, UK). X-ray diffraction (XRD) spectra were taken with a Miniflex II (Cu K_α radiation, Rigaku Americas, The Woodlands, TX) on a galvanic electrode ($w \approx 50$ μm, $s \approx 50$ μm) before and after $\approx$45 min of reaction time with pH 3 HCl in order to obtain sufficient amounts of material for analysis.

Experiments assessing the degree of particle adherence, as particle concentration was increased, were conducted in an "open drop" galvanic cell. Galvanic electrodes with the geometry $w \approx 50$ μm, $s \approx 950$ μm, and $h \approx 37$ nm were used. The reactions were started by pipetting 40 μL of PS suspension in pH 3 HCl solution onto the galvanic electrode. The resulting hemispherical suspension droplet had a height of $d \approx 2$ mm. Following about 40 min of reaction time, the electrodes were immersed in DI water, swirled for $\approx$10 s, and gently dried with a stream of nitrogen gas. Afterward, the electrodes were examined using bright-field optical microscopy.

RESULTS AND DISCUSSION

To determine the onset of colloidal particle cementation in the microreactor, we performed in situ particle tracking of PS microspheres on the copper electrodes. This was done for different thicknesses of the copper electrodes, so that the amount of RPs generated as a result of copper dissolution would be varied. We also monitored the discoloration of the dissolving copper electrodes, which could be an indicator of the formation of insoluble RPs.[26,27]

Effect of Anode Thickness on Colloidal Dynamics. Figure 2a−c shows time-lapse images of the PS particle aggregation process on copper electrodes with three different thicknesses h (data available as video sequences in the Supporting Information, videos 1−3). Distinct stages of particle motion are observed during the course of the experiments, as indicated by roman numerals next to the time-lapse images in Figure 2a−c: (I) Initially, single particles that have been transported to the copper anode by directed long-range flow and electrophoresis[14,15] display motion as singlets on the anode for less than a minute. (II) As the number density of singlets increases over time, crystalline rafts nucleate and grow by incorporating singlet particles and by merging with neighboring rafts. During this process, the rafts continue to display a net motion on the anode, and lattice vibrations within the rafts allow for annealing into single crystalline structures.[14,15] (III) After a few minutes, the rafts redisperse in the case of small and intermediate h. In Figure 2b,c, a fourth stage (IV) is observed: rafts as well as singlets eventually become immobile on the surface.

We quantified the motion of the particles with the projected displacement Δx during a time interval of Δt = 1 s for a representative colloidal particle for each of the three values of h (Figure 2d). For all values of h, in Stage I, we observe large particle displacement Δx in excess of 1.5 μm, as the tracked PS particles are initially transported toward the copper electrode and exhibit directed motion toward other particles on the electrode due to electrokinetic effects, as detailed elsewhere.[7,14,15,17] In Stage II, a rapid drop in Δx below that of a Brownian particle (Δx_{diff} = 0.86 μm, with D = 0.19 $\mu m^2/s$, determined from the Stokes−Einstein equation) is observed as crystalline rafts form, merge, and display annealing dynamics, since the tracked particles are now confined within a raft, and thus, their net motion cannot be larger than that of the raft.

For the microreactor with the smallest value of $h \approx 26$ nm (Figure 2a), during Stage II, Δx fluctuates around a value of 0.25 μm (blue curve in Figure 2d). The raft remains mobile as a whole, which gives rise to the jump at $t \approx 250$ s when the aggregate significantly shifts its position. Stage III begins at $t \approx 300$ s, when we first observe a gradual increase in lattice vibration (see Supporting Information video 1) until, eventually, the particles begin to disperse into the bulk electrolyte, as seen by the gradual increase of Δx. Δx eventually reaches the value of Δx_{diff}, around which it fluctuates with a high amplitude due to the random (i.e., Brownian) nature of the particle motion. Less than 5% of the PS particles do not redisperse and remain attached to the electrode, but they can be easily removed by the postreaction rinsing and drying procedure.

For the microreactor with $h \approx 32$ nm (Figure 2b, Supporting Information, video 2), particles remain aggregated for a longer period of time in Stage II compared to the case with $h \approx 26$ nm. For most of the duration of this extended Stage II, the displacement of the corresponding tracked particle (black curve in Figure 2d) is lower compared to the previous case, indicating stronger confinement and decreased raft mobility. Particle dispersion at $t \approx 365$ s (beginning of Stage III) is characterized by a more sudden increase in particle surface diffusion than in the previous case. By $t \approx 397$ s, no crystalline patches are present any more. Shortly after, at $t \approx 429$ s (onset of Stage IV), all particles immobilize within a few seconds. Particle displacement drops to the noise level, and the disordered configuration of the particles obtained as a result of the intermittent period of surface diffusion is retained until the termination of the experiment. However, the redispersed and subsequently immobilized PS particles do not resist rinsing and drying after experiment termination.

With a large $h \approx 61$ nm (Figure 2c), more than 90% of the first layer particles never redisperse after they have formed aggregates on the copper electrode; instead, they remain within close-packed, mostly crystalline aggregates and resist rinsing and drying after experiment termination. The displacement of the tracked particle (which becomes part of a large raft early in the experiment) consequently remains at the noise level until experiment termination, and we are unable to detect the onset of Stage IV. However, we also observe that, by $t \approx 650$ s, a small number of second layer particles (aggregated on top of the first colloidal particle layer) begin to redisperse, and additional PS particles arriving on the electrode through sedimentation no longer exhibit directed motion towards rafts (Supporting Information video 3, and Figure 2c). These observations indicate that electrochemical copper dissolution has ceased by then. At the same time, it can be seen in the corresponding video sequence (Supporting Information video 2) that also a minority (<10 %) of the first layer particles located at the edges of the rafts as well as those participating in smaller rafts exhibit increased lateral vibration and redispersion (Stage III), which is followed by immobilization at $t \approx 760$ s (Stage IV), analogous to the colloidal dynamics observed in the $h \approx 32$ nm microreactor. These particles have arrived at the copper electrode at a later stage of the experiment; that is, they have been in contact with the dissolving copper electrode for a shorter time. Thus, particles that arrive on the electrode at an early stage of the experiment and thereby are located at the centers of the larger rafts experience immobilization already during Stage II while they are being constrained within the rafts by electrokinetic effects. On the other hand, particles that arrive later at the electrode and are thereby located at the edges of the rafts are immobilized after a brief period of redispersion. This implies that not only changes of the electrode surface but also changes of the PS particle surface occurring over time play a role in particle immobilization. Factors leading to such changes are discussed in the following.

The immobilization events for $h \approx 32$ and 61 nm mark the point where a transition from repulsive (particles mobile) to attractive (particles immobilized) particle−substrate interactions occurs. Such a transition can be effected by a variety of phenomena. Its dependence on the amount of copper in the system as well as on reaction time suggests that gradual changes in the microreactor chemistry occurring as a result of the electrochemical reactions have an effect on the nature of the PS surface, the electrode, or both, leading to a change in the substrate−particle interactions. In the case of $h \approx 61$ nm, strong discoloration occurs during the dissolution of the copper film (Figure 2c), which we have previously shown to be indicative of RP deposition or precipitation.[26,27] RPs on the PS or the substrate surfaces can alter the substrate−particle interaction by affecting the electrostatic repulsive forces or the strength of the van der Waals attraction. The magnitude of the forces may also vary due to closer contact with the substrate as the RPs nucleate and grow at the particle−substrate contact regions (Figures 1c and 2c of ref 14).

To discern the potential impact of these different factors, we probed the stability of the colloidal dispersion during particle aggregation by employing nearly twice the particle concentration in comparison to the experiments summarized in Figure

2 in a microreactor with copper electrodes of about 80 nm in thickness. As shown in Figure 3, in this case, multiple layers of

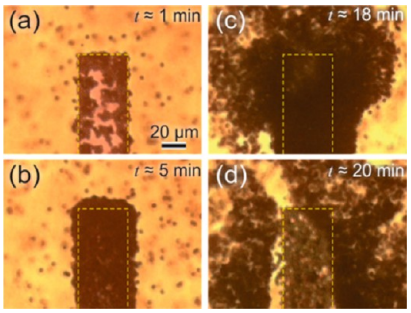

Figure 3. Time-lapse in situ images of the tip of a copper electrode ($w \approx 40$ μm, $s \approx 140$ μm) during a reaction with a suspension of 2.3 μm PS particles (0.015 vol %) in pH 3 HCl electrolyte. (a, b) PS aggregating and accumulating on the copper electrode to form multiple layers of colloidal aggregates. (c, d) Layers above the first monolayer disperse into the electrolyte while the first monolayer remains on the electrode surface. This monolayer of colloidal particles remains adherent to the substrate and is resistant to the rinsing and drying procedure. The dashed lines mark the initial border of the copper electrode.

aggregated colloidal particles cover the electrode during corrosion of the copper electrode. After a period of time, the accumulated colloidal particles begin to diffuse away from the electrode surface and disperse into the electrolyte, with the exception of a particle monolayer that adheres to the electrode and is resistant to rinsing and drying. The redispersion of the colloidal particles suggests that the particles remained charge-stabilized throughout the experiment despite the increasing ionic strength due to accumulating soluble RPs. Therefore, it is unlikely that the adhesion of the first monolayer is caused by a loss of colloidal stability (i.e., by a decrease in repulsion between the substrate and the first PS particle layer due to changes in electrolyte composition). Further, the electrokinetic forces cannot be responsible for pushing the particles into the primary minimum of the electrode−colloid interaction potential because we observe in the $h \approx 32$ nm microreactor that particle immobilization (Stage IV) follows the termination of electrokinetic activities (Stage III). Rather, the event leading to particle immobilization must be associated with other chemical processes in the microreactor, such as the cementation of the colloidal particles by precipitation and deposition of insoluble RPs. To investigate how precipitated or deposited RPs affect particle adhesion, in the next section, we present the changes on the substrate surface during the reactions due to RP deposition and put them in relation to the different stages of particle motion described above.

Effect of Anode Thickness on RP Deposition. Figure 4 shows the evolution of the color signal[26] from the copper region C_{Cu} and the gold region C_{Au} of the galvanic electrode with different h (corresponding to the microreactors in Figure 2). Initially, copper and gold regions show distinct signals, corresponding to the visually different color of the two metals under the optical microscope. For the smallest value of h (≈26 nm), C_{Cu} decreases monotonously with time, until, at $t \approx 250$ s, it reaches the value of C_{Au} (≈0.48) and plateaus. During that process, C_{Au} shows a small decrease as well. The continuous decrease of C_{Cu} is predominantly associated with the thinning of the copper film, that is, its increasing optical transparency

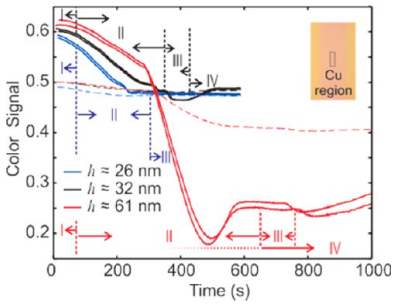

Figure 4. Time progression C_{Cu} (solid lines) and C_{Au} (dashed lines) for galvanic electrodes with varying h. Other reactor dimensions (see Figure 1a) are kept constant: $w \approx 50$ μm, $s \approx 950$ μm, and $d \approx 350$ μm). We display C_{Cu} from two experiments for every h, and minor discrepancies between the curves reflect measurement variations between experiments and slight differences in the geometry of the electrodes during microfabrication procedure. For clarity of the figure, we exhibit only one C_{Au} for each h. Boundaries between stages of PS particle motion as defined in Figure 2 are indicated by dashed vertical lines.

during dissolution until eventually all copper is dissolved.[26] This point marks the termination of any electrokinetic activity in the microreactor and roughly corresponds to the observed transition of colloidal dynamics from Stage II to III (Figure 2a,d), where particle redispersion could be noticed around $t \approx 300$ s. The small drop in C_{Au} is likely associated with the formation of minute amounts of insoluble RPs on or near the electrode giving rise either to increased roughness of the originally mirror-like gold surface or to scattering within the electrolyte, thus deflecting light out of the imaging path. To a small extent, RPs may contribute to the change in C_{Cu} as well.

For intermediate h (≈32 nm), the initial changes in C_{Cu} and C_{Au} resemble our observations for the $h \approx 26$ nm case. However, after reaching C_{Au} and remaining there from $t \approx 330$ to 350 s, C_{Cu} begins to drop below C_{Au}, which is indicative of the formation of insoluble RPs.[26,27] At $t \approx 370$ s, C_{Cu} plateaus at a value of 0.47 for about 60 s, suggesting that there is no more net increase in RP amount, before rising slowly, crossing the gold value of about 0.48 at $t \approx 480$ s and finally remaining at a slightly larger value of 0.49 until experiment termination. The variation of C_{Cu} after $t \approx 370$ s indicates that the nature of the RPs on the copper region changes in time after the electrochemical dissolution of copper has stopped. C_{Cu} can potentially be affected by variations in the morphology of the electrode surface (light scattering on the electrode substrate), by varying amounts of suspended precipitants in the electrolyte (light scattering in the electrolyte above the substrate), or by changes in the intrinsic optical properties of the substrate (due to chemical changes). Thus, the observed final change in C_{Cu} could be caused by a change in the size of deposited RP particles, the deposition of initially suspended RP precipitates, the chemical conversion of the RP, for example, from a copper chloride to a copper oxide species (see below), or the dissolution of initially deposited RPs. Because we are not able to assess the structure of the RP in situ to such a level of detail, we cannot determine which of these effects gives rise to the increase in C_{Cu} around $t \approx 480$ s. The observation that the final value of C_{Cu} differs from C_{Au} suggests that RPs remain present. Thus, we contend that the final change in C_{Cu} is due to a chemical or morphological change in the RP and not due to its dissolution.

dx.doi.org/10.1021/am4014117 | ACS Appl. Mater. Interfaces 2013, 5, 6346−6353

When we compare the dynamics of the observed color changes in the case of $h \approx 32$ nm with the corresponding particle aggregation dynamics (Figure 2b,d), we find that particle redispersion (Stage III) coincides with C_{Cu} dropping below C_{Au} and that immobilization (Stage IV) appears to be associated with the following rise in C_{Cu}. Therefore, particle immobilization appears not to be the immediate result of the occurrence of insoluble RPs. Rather, subsequent processes, for example, the deposition of precipitates or the chemical conversion of RP deposits, cause the PS particles to experience attractive interactions with the substrate and to stick. These final RP deposits thus are responsible for "cementing" the colloidal particles to the electrode substrate.

For $h \approx 61$ nm, C_{Cu} begins to drop quickly already at ≈290 s, before it reaches the value of C_{Au} at $t \approx 324$ s. By this time, also C_{Au} begins to decrease significantly. These drops in color signal indicate the early onset of RP deposition on both locations. Both C_{Cu} and C_{Au} continue to decrease until $t \approx 490$ s, when C_{Cu} reaches a minimum of ≈0.2 and C_{Au} begins to plateau at a value of 0.41, significantly below the final value of C_{Au} observed for the thinner copper electrodes. Within the next 60 s, C_{Cu} increases up to 0.25, where it remains for a few minutes until further variations occur at $t \approx 800$ s. We suspect that the observed minimum in C_{Cu} corresponds to the brief drop in C_{Cu} seen for $h \approx 32$ nm between $t \approx 370$ s and $t \approx 430$ s. With the thicker copper film, however, a larger amount of insoluble RPs forms so that the effect is much stronger and that the substrate changes color not only on the copper region but also on the gold. Because of the absence of redispersion in the particle tracking data, we can only hypothesize that PS particle immobilization is likely to occur during the rise of C_{Cu} after $t \approx 490$ s. Consistent with our prior findings that the RP at the end of the reactions is predominantly Cu_2O,[14] ex situ examination of electrodes containing large amounts of deposited RPs by EDS indicates that there is increased oxygen content on the copper region. In addition, a $Cu_2O(111)$ diffraction peak also emerges from the XRD spectra following the reactions (see the Supporting Information).

The dependence of particle cementation and RP deposition on the copper amount and reaction times suggests that the transport and accumulation of soluble RPs in the electrolyte play a role. To test the contribution of the soluble RP concentration, we increased the electrolyte depth of the experiment in Figure 2b ($h \approx 32$ nm) by a factor of ≈1.5. As a result of increased electrolyte volume, particle immobilization (Stage IV) no longer occurs. Colloidal particles redisperse and behave similarly to the microreactor with small h shown in Figure 2a. This confirms that a threshold concentration of soluble RPs is required for particle cementation, which is consistent with our assessment that particle cementation is induced by RP deposition. In the following, we determine the type of RP involved in particle cementation and how RP formation and particle cementation are affected by changing electrolyte concentrations during the copper corrosion processes.

Chemical Processes and Chemical Phase Equilibria. During the corrosion of copper in aqueous chloride media, RPs can be expected to change from an initial CuCl film to the precipitation of Cu_2O and/or other species, including $Cu_2(OH)_3Cl$, as the concentration of ionic species in the electrolyte changes.[18,20−22] While the formation of many RP species is affected by chloride concentration, only some RP precipitates, including Cu_2O and $Cu_2(OH)_3Cl$, are directly influenced by the electrolyte pH. To distinguish the contribution of the two types of RPs on particle cementation, we looked for changes in RP formation and particle dynamics at increased initial pH. To this end, we used a microreactor geometry identical to that shown in Figure 2a, which, at a pH of 3, had insufficient copper to form RPs or cement colloidal particles.

As we increase the initial pH to 3.5 while maintaining a 1 mM chloride concentration by addition of sodium chloride (NaCl), we observe a similar drop in C_{Cu}, as seen in the $h \approx 61$ nm microreactor at pH 3 (Figure 4), indicating RP deposition (see Figure 5a). Furthermore, PS particles become cemented to the copper area such that they are resistant to postreaction rinsing and drying (Figure 5b,c). To discern the contribution of chloride concentration, we conducted another experiment with pH 3.5 HCl only, that is, without added NaCl. In this experiment, we again observe RP deposition, as indicated by the sharp drop in C_{Cu} (Figure 5a), as well as the formation of cemented particles (Figure 5d,e). Compared to the experiment with added NaCl, however, RP deposition occurs about 90 s later, which is likely due to slower electrochemical dissolution kinetics as a result of the lowered chloride concentration.[18,20,21] We notice that the final differences between C_{Cu} and C_{Au} in the two experiments are approximately the same, indicating that similar amounts of RPs have been deposited. This shows that chloride concentration affects mostly the rate of copper

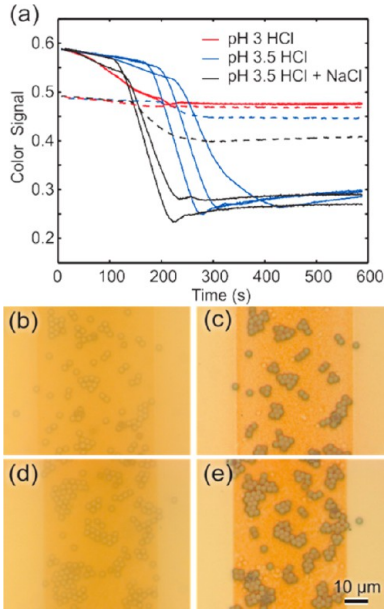

Figure 5. RP formation and particle adherence in a galvanic microreactor with a thin Cu film ($h \approx 26$ nm) and different pHs and chloride concentrations. (a) The time progression of C_{Cu} (solid lines) and C_{Au} (dashed lines) during reactions with different electrolytes. C_{Cu} from three experiments conducted with pH 3.5 HCl electrolyte and two experiments each for pH 3 HCl electrolyte (control experiment) and pH 3.5 HCl with added NaCl to adjust for 1 mM chloride content are shown to demonstrate experimental variations. For clarity of the figure, we exhibit only one C_{Au} for each experimental condition. (b−e) PS particle distributions after reactions with a suspension of 2.3 μm PS particles in (b, c) pH 3.5 HCl with added NaCl to adjust for 1 mM chloride content, and (d, e) pH 3.5 HCl only. Images are taken in situ just before reaction termination (b, d), and after rinsing and drying (c, e).

dx.doi.org/10.1021/am4014117 | ACS Appl. Mater. Interfaces 2013, 5, 6346−6353

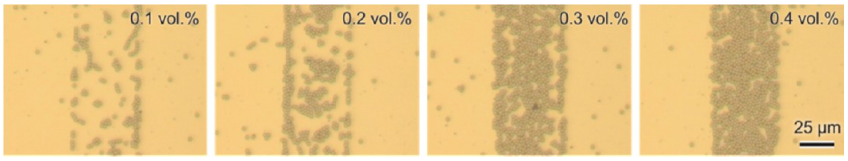

Figure 6. Optical images of the rinsed and dried galvanic electrode following reactions with a free-standing droplet (40 μL) of a pH 3 HCl suspension containing varying PS particle concentrations. The drop height is ≈2 mm. Other microreactor parameters are kept constant: $w \approx 50$ μm, $s \approx 950$ μm, $h \approx 37$ nm.

dissolution, as described by eqs 1 and 2, leading to a faster accumulation of soluble RPs and an earlier onset of insoluble RP deposition, that is, Cu_2O. Meanwhile, electrolyte pH and copper amount determine the thermodynamic stability and total amount of RPs, such as Cu_2O. Because elevating the initial pH alone, that is, without changing the initial chloride concentration, induces the cementation of PS particles, we contend that primarily the deposition of RPs forming in response to an elevated pH (e.g., Cu_2O and $Cu_2(OH)_3Cl$) effects particle cementation.

The order of magnitude of the pH increase necessary to deposit sufficient amounts of RP for particle cementation can be roughly estimated by calculating the reactor-intrinsic pH changes for the microreactor with the intermediate electrode thickness shown in Figure 2b since it exhibits the onset of RP deposition and only weak PS cementation. Since cementation follows shortly after the complete dissolution of the copper film, we calculate the minimum pH increase at the end of the experiment, when the electrolyte can be considered well-mixed by diffusive transport. For illustration purposes, we conduct our calculations based on chemical processes leading to Cu_2O precipitation (see Supporting Information for assumptions made in the calculations). A similar analysis can also be conducted for other RPs affected by pH based on their specific chemical processes. We assume that the reduction reaction according to eq 5 fully balances cupric ion formation (eqs 1−3) while both copper dissolution via the $CuCl_2^-$ pathway (eqs 1−2) and the Cu_2O deposition reaction (eq 4) run to completion (i.e., all copper is reacted away). We find that Cu_2O precipitation is accompanied by a rise in pH to a value of ≈3.15. Therefore, by "artificially" increasing the initial pH, as we did in the experiment shown in Figure 5, a pH suitable for Cu_2O formation and particle cementation was already met at the beginning of the experiment, resulting in the deposition of large amounts of RPs.

In the presence of colloidal aggregates, in particular, of particle multilayers, the assumption that the system is well-mixed is only a poor approximation, as concentrations near the electrodes may locally be altered by the aggregated colloidal particles acting as diffusion barriers. Indeed, such effects can create locally favorable conditions for RP precipitation, as we can demonstrate with an experiment conducted in an open drop configuration with increased electrolyte volume with $d \approx 2$ mm (Figure 6). Here, the global pH as well as the concentration of copper ions in solution cannot reach the necessary value for RP formation if the electrolyte is well-mixed. However, we still observe the formation of cemented colloidal particles, as can be seen in the figure. To investigate this further, we studied the effect of varying PS particle concentrations on cementation. We varied the PS particle concentration between 0.1 vol %, where the copper electrode becomes fully covered by a monolayer of PS particles during the course of the experiment, and 0.4 vol %, at which the copper area is quickly covered by a particle multilayer in situ. An assessment of the electrodes following reaction, rinsing, and drying shows that the number density of cemented PS microspheres on the copper region increases with increasing particle concentration in the electrolyte. This suggests that the presence of particle multilayers during the dissolution reaction causes a local change in electrolyte composition, for example, an increase in pH and copper ion concentration, such that conditions are more favorable for RP precipitation and deposition.

CONCLUSIONS

We determined the onset of cementation of polystyrene colloidal particles in a Cu−Au galvanic microreactor onto the electrode substrate and related this event to the chemical processes taking place in the system. To enable a precise correlation, we tracked the motion of colloidal particles on corroding copper electrodes while simultaneously monitoring the copper dissolution dynamics as well as the occurrence of insoluble RPs on the electrode surface. By tuning the amount of copper, we determined the time at which the immobilization occurred as well as the strength of the substrate−particle bond (determined qualitatively by assessing the resistance of cemented colloidal aggregates to rinsing). With an insufficient amount of copper in the reactor, insoluble RPs, such as cuprous oxide, did not precipitate, and after the copper was dissolved, colloidal particles redispersed into the electrolyte. By increasing the amount of copper or by raising the pH of the electrolyte, insoluble RPs precipitated and colloidal particles stuck to the electrode substrate once a critical threshold in RP solubility and pH was exceeded.

We rule out electrokinetic effects or the loss of colloidal stability as the causes of particle immobilization as the particle cementation is initiated at a later stage of the copper corrosion process and colloidal multilayers on the electrode remain colloidally stable. Since particle aggregation (effected by electrokinetics) and cementation are thus separate processes, colloidal rafts on the electrode can "anneal" into single crystalline structures before immobilization sets in if parameters are chosen such that immobilization is sufficiently delayed to allow for such "annealing" to take place.

ASSOCIATED CONTENT

Supporting Information

Corresponding videos for the image sequences in Figure 2a−c, XRD spectrum indicating $Cu_2O(111)$ peak in reacted electrodes, and assumptions and calculations used for evaluating minimum increase in pH. This material is available free of charge via the Internet at http://pubs.acs.org.

AUTHOR INFORMATION

Corresponding Author

*E-mail: iaksay@princeton.edu.

Notes

The authors declare no competing financial interest.

■ ACKNOWLEDGMENTS

This work was supported by the ARO/MURI under grant number W911NF-04-1-0170, and NASA University Research, Engineering, and Technology Institute on BioInspired Materials (BIMat) under Award No. NCC-1-02037. C.P. acknowledges partial financial support from the Alexander von Humboldt Foundation.

■ ABBREVIATIONS

DI, deionized
EDS, energy-dispersive X-ray spectroscopy
PDMS, poly(dimethylsiloxane)
PS, polystyrene
RP, reaction product
SEM, scanning electron microscopy
XRD, X-ray diffraction

■ REFERENCES

(1) Baksh, M. M.; Jaros, M.; Groves, J. T. *Nature* **2004**, *427*, 139−141.
(2) Ben-Moshe, M.; Alexeev, V. L.; Asher, S. A. *Anal. Chem.* **2006**, *78*, 5149−5157.
(3) Holtz, J. H.; Asher, S. A. *Nature* **1997**, *389*, 829−832.
(4) Vlasov, Y. A.; Bo, X. Z.; Sturm, J. C.; Norris, D. J. *Nature* **2001**, *414*, 289−293.
(5) Cui, Y.; Bjork, M. T.; Liddle, J. A.; Sonnichsen, C.; Boussert, B.; Alivisatos, A. P. *Nano Lett.* **2004**, *4*, 1093−1098.
(6) Rinne, S. A.; Garcia-Santamaria, F.; Braun, P. V. *Nat. Photonics* **2008**, *2*, 52−56.
(7) Trau, M.; Saville, D. A.; Aksay, I. A. *Science* **1996**, *272*, 706−709.
(8) Yeh, S. R.; Seul, M.; Shraiman, B. I. *Nature* **1997**, *386*, 57−59.
(9) Ramos, A.; Morgan, H.; Green, N. G.; Castellanos, A. *J. Phys. D: Appl. Phys.* **1998**, *31*, 2338−2353.
(10) Hayward, R. C.; Saville, D. A.; Aksay, I. A. *Nature* **2000**, *404*, 56−59.
(11) Velev, O. D.; Bhatt, K. H. *Soft Matter* **2006**, *2*, 738−750.
(12) Ristenpart, W. D.; Jiang, P.; Slowik, M. A.; Punckt, C.; Saville, D. A.; Aksay, I. A. *Langmuir* **2008**, *24*, 12172−12180.
(13) Kline, T. R.; Iwata, J.; Lammert, P. E.; Mallouk, T. E.; Sen, A.; Velegol, D. *J. Phys. Chem. B* **2006**, *110*, 24513−24521.
(14) Punckt, C.; Jan, L.; Jiang, P.; Frewen, T. A.; Kevrekidis, I. G.; Saville, D. A.; Aksay, I. A. *J. Appl. Phys.* **2012**, *112*, 074905.
(15) Jan, L.; Punckt, C.; Khusid, B.; Aksay, I. A. *Langmuir* **2013**, *29*, 2498−2505.
(16) Ristenpart, W. D.; Aksay, I. A.; Saville, D. A. *J. Fluid Mech.* **2007**, *575*, 83−109.
(17) Böhmer, M. *Langmuir* **1996**, *12*, 5747−5750.
(18) Braun, M.; Nobe, K. *J. Electrochem. Soc.* **1979**, *126*, 1666−1671.
(19) Faita, G.; Fiori, G.; Salvadore, D. *Corrosion Sci.* **1975**, *15*, 383−392.
(20) Kear, G.; Barker, B. D.; Walsh, F. C. *Corrosion Sci.* **2004**, *46*, 109−135.
(21) Lee, H. P.; Nobe, K. *J. Electrochem. Soc.* **1986**, *133*, 2035−2043.
(22) Bianchi, G.; Longhi, P. *Corrosion Sci.* **1973**, *13*, 853−864.
(23) Genshaw, M. A.; Damjanov., A.; Bockris, J. O. *J. Electroanal. Chem.* **1967**, *15*, 163−172.
(24) O'Brien, R. W.; White, L. R. *J. Chem. Soc., Faraday Trans. 2* **1978**, *74*, 1607−1626.
(25) Savitzky, A.; Golay, M. J. E. *Anal. Chem.* **1964**, *36*, 1627−1639.
(26) Punckt, C.; Aksay, I. A. *J. Chem. Phys.* **2009**, *131*, 244710.
(27) Murira, C. M.; Punckt, C.; Schniepp, H. C.; Khusid, B.; Aksay, I. A. *Langmuir* **2008**, *24*, 14269−14275.